Fault Diagnosis of an Automobile Cylinder Block with Neural Process of Modal Information

Morteza Mohammadzaheri*, Amirhosein Amouzadeh,
Mojtaba Doustmohammadi, Mohammadreza Emadi, Navid Nasiri
Sultan Qaboos University, Oman
*morteza@squ.edu.om and mmzahery@gmail.com

Ehsan Jamshidi

Energy and Sustainable Development Research Center, Semnan Branch, Islamic Azad University, Semnan, Iran

Mojtaba Ghodsi

University of Portsmouth, UK

Payam Soltani

Birmingham City University, UK

***Abstract*— The focus of this article is fault-diagnosis of complex mechanical parts through the process of their modal information using a multi-layer perceptron (MLP), a type of artificial neural networks (ANNs). The major contribution of this work is to formulate the problem of fault diagnosis of complex mechanical parts based on their modal information so as to be solved with use of ANNs. This method consists of three major steps: (1) Extracting natural frequencies of the part with or without faults. (2) Creating the "fault signatures" by deducting the natural frequencies of some faulty specimens from the ones of the faultless part. (3) Constructing and training a mathematical model in the form of an ANN, with information obtained in previous steps, to locate (and even further characterize) the fault. The presented method was successfully adopted to estimate the location of an under-surface mechanical fault on an automobile cylinder block and is shown to have the potential to solve more sophisticated fault diagnosis problems.**

***Index Term*— Vibrations; Fault Diagnosis; Natural Frequencies; Artificial Neural Networks; Cylinder Block**

1. INTRODUCTION

Fault diagnosis, as a key concept in different areas technology [1-6], may answer a number of the following three critical questions: (i) is there any faults? i.e. fault detection, (ii) where is (are) the fault(s)? i.e. fault isolation, (iii) how is the fault? (e.g. in terms of size and shape) i.e. fault identification [7, 8].

In some fault diagnosis methods, the response/information of a healthy system is evident; for instance, a metal part with no holes allows an ultrasonic wave to pass at a certain speed, as an evident response of a healthy system. In these so called 'signal-based' methods, only the response/information of the faulty system is utilised for fault diagnosis[7, 9]. In other fault diagnosis methods, a model or some behavioural information of the healthy system should be used for fault diagnosis. Such methods are called 'model-based', e.g. vibration-based fault diagnosis of mechanical structures, which need some information about the healthy system for fault diagnosis [10, 11].

Fault diagnosis is currently employed and/or explored for different systems such as chemical processes [12], electric motors [13] and mechanical structures [14]. Both signal-based and model-based techniques are used for fault diagnosis of mechanical parts/ structures, also known as structural damage detection. At the moment, signal-based methods such as radiography, ultrasonic, use of magnetic and thermal fields, CT scanning and eddy-current techniques are extensively employed in structural damage detection [9, 15, 16]. Inasmuch as all these techniques should be used in the locality of the fault [15], *local* damage detection is almost an equivalent of signal-based fault diagnosis [17]. On the contrary, model-based vibrational fault diagnosis techniques use the modal/dynamic properties of the 'whole' system; therefore, these methods are considered *global*. In other words, vibration-based methods do not depend on the data gathered from the fault locality. As a result, terms 'global' and 'model-based' are exchangeably used in the literature of structural damage detection [11].

Ideally, vibration-based methods can provide information on damage existence (fault detection), location (fault isolation) and size for a mechanical structure (fault identification) [18]. The reliability of vibration-based approach convinced NASA, in the late 1980s, to employ this approach to inspect its shuttle instead of prevalent signal-based methods [19]. This approach was, and is still mostly, seen as fault diagnosis on the basis of dynamic/modal properties of mechanical structures [9, 18,

20-23]. Natural frequencies, mode shapes and damping ratios are dynamic/modal properties widely used for this purpose [18]. Obtaining meaningful fault diagnosis information out of these modal properties is a major task in vibration-based fault diagnosis approaches.

Some research disappointingly concluded that only higher frequency modes (e.g. with natural frequencies over 30 kHz) are sufficiently sensitive to local defects [15]; while, prevalent acceleration sensors work at frequencies up to 10 kHz which can investigate modes with below 5 kHz natural frequencies [24]. That is, expensive vibration sensors with demanding operations may be needed to obtain meaningful vibrational information for fault diagnosis. This disappointing conclusion faded the initial hopes to extensive use of vibration-based methods in quality control of manufactured metal parts [15]. This research re-formulates vibration-based fault diagnosis problem so as to employ artificial intelligence to extract meaningful results out of low frequency vibrational modal information of a complex mechanical part. This work is inspired by recent sparse applications of artificial intelligence (AI) techniques to process vibrational information for fault isolation purposes [10, 11, 18, 25] (the employed technique is essentially different from feature classification e.g. [26]). The proposed method has been successfully adopted and tested for isolation of a fault on an automobile cylinder block, a structure with a complex geometry.

2. Proposed MEthod and its Deveopment Steps

The developed fault diagnosis algorithm receives natural frequencies (extendible to other modal information) of a complex mechanical structure (an automobile cylinder head, in this research), belonging to low frequency (<5kHz) modes, and provide its fault information (fault location, in this research).

Three following steps should be taken to develop the proposed method:

(1) Modal analysis of the part without or with faults to find the natural frequencies associated with each healthy or faulty specimen. Section 4 details this step for the case study of this paper.

(2) Pre-process of information collected at Step 1 to produce “fault signatures”. This stage, for the automobile cylinder block, is presented in section 5.

(3) Creating a mathematical model in the form of a multilayer perceptron and training the data obtained at Step 2 to this model. The inputs to the model are the elements of the fault signature vector, and the output is (are) the location (and potentially other characteristics) of the fault (s). This step is presented in section 6.

3. Case Study

The case study is a cylinder block of an automobile engine made by SAIPA, an Iranian car manufacturer, depicted in Fig.1. High level of thermomechanical stress on the top surface of the cylinder block during operation of the engine makes this component very sensitive to the existence of any mechanical faults.

The part, assumingly, may have one fault happening at different spots on a line, depicted in Fig. 2. The fault is a spherical void with the diameter of 1cm, situated 2.5 cm underneath the top surface, a common size and depth for casting faults [27]. A point highlighted in red (2.5 cm far from the edge) in Fig.2 is considered as the origin; the distance of fault centre to the origin is assumed as the fault location. For development and validation of the proposed method on the case study, modal information of the healthy cylinder block and 20 faulty specimens, with fault locations depicted in Fig. 2, one per specimen, was employed. Location of the closest fault to the origin is considered as fault location 1, and others as fault locations 2, 3, … , 20 as they are located further form the origin.

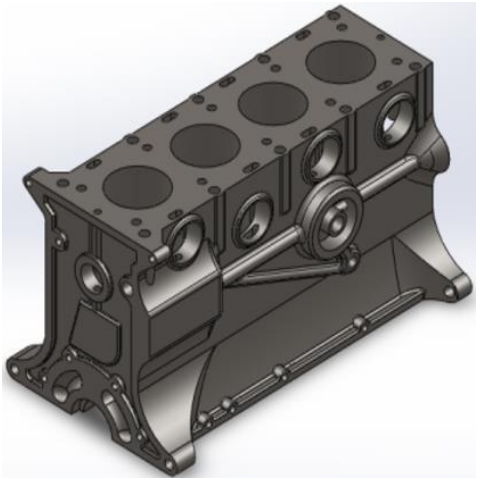

Fig. 1. A 3D geometrical model of the cylinder block

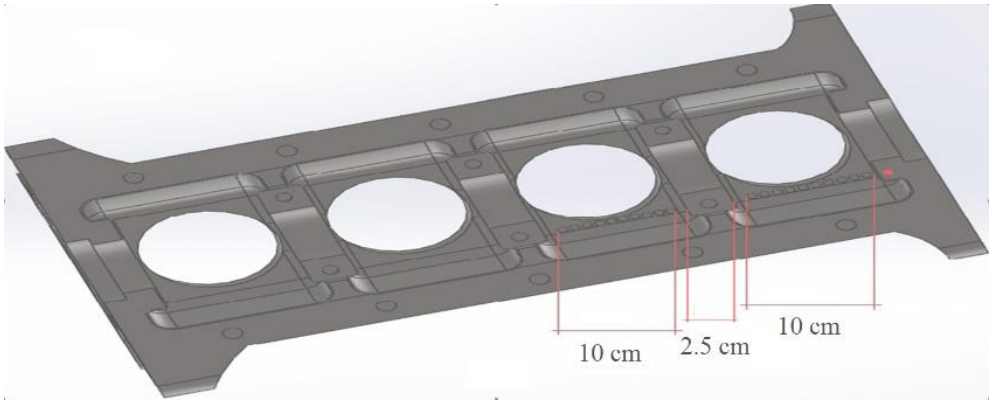

Fig. 2. Fault locations on the top surface of the cylinder block. The red point is the origin

4. STEP1- MODAL ANALysis.

Due to experimentation limits, a finite element model (FEM) of the cylinder block was first developed and experimentally validated. Then, a fault was added to the validated FEM, at locations depicted in Fig.2, one at a time. Natural frequencies of faulty specimens were calculated through numerical simulation using the validated FEM.

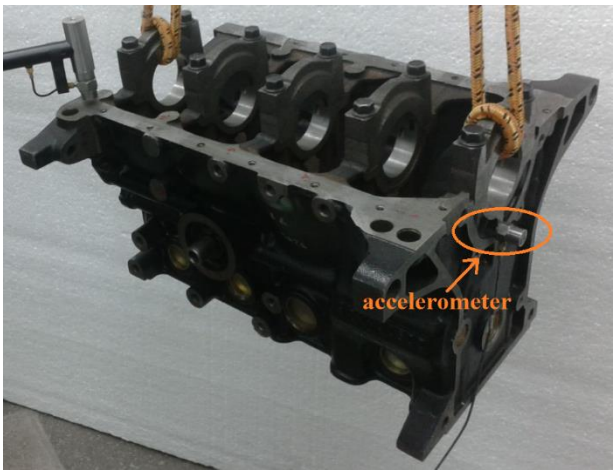

Fig. 3. Experimental Modal Analysis, the cylinder block is hanged upside down.

The FEM of the cylinder-block is made up of 2002793 nodes and 1179381 irregular Tetrahedral element, constructed in ANSYS 14.0 software package. For model validation purposes, a standard experimental modal analysis was performed on the case study as shown in Fig.3.

In experimental modal analysis, the acceleration of a point on the structure (indicated in Fig.3 within a red ellipse) was measured and recorded with a A/120/V DJB single-axis integrated-electronics piezoelectric accelerometer; while, 8202 B&K impact hammer hit 21 different points on the structure on by one. A B&K 3560 analyzer was employed to extract modal properties of the case study.

Natural frequencies resulting from the FEM and experimental modal analysis, presented in Table 1, clearly demonstrate the accuracy of the FEM, where

$$\text{difference}\% = \frac{|\text{experimental natural freq-FEM natural freq}|}{\text{experimental natural freq}} \times 100.$$

5. Step 2- Pre-process of Vibrational Data

Modal analysis of the healthy specimen, as detailed in section 4, resulted in an array of its first 24 vibrational modes with natural frequencies below 5 kHz. These 24

Table I
Natural frequencies resulting from experimental and FEM modal analysis.

Mode No.	FEM Natural Frequency (Hz)	Experimental Natural Frequency (Hz)	Difference%
1	1234.4	1239.7	0.4
2	1660.3	1653.6	0.4
3	2364.6	2375.9	0.5
4	2705	2698.4	0.2
5	3068.2	3071.4	0.1

natural frequencies are presented as ω_i. i indicates vibrational mode, an integer in the range of [1 24]. Faulty specimens were simulated using the validated FEM and went through numerical modal analysis, leading to 24 below 5 kHz natural frequencies of ${}_k\omega_i$, where k refers to the fault location. Thus, k is an integer in the range of [1 20]. It should be noted that the sole reason for use of FEM is experimentation limits. In the case of availability of faulty specimens, this method can be conducted using experimental modal analysis instead.

After finding natural frequencies of healthy and faulty specimens, all the natural frequencies of faulty specimens were deducted from the natural frequencies of the healthy part. The result is an array of 24 numbers for each fault location. This array is called the '*signature of fault location*' or in short '*fault signature*', ${}_k\mathbf{M}$, for k[th] fault location. For mode i and fault location of k:

$$ {}_k\mathbf{M}_i = {}_k\omega_i - \omega_i . \quad (1)$$

In total, 20×24=480 samples of data are the outcome of this step. Table 2 presents the first ten natural frequencies and the first ten elements of the fault signature for the first fault locations, the closest to the origin in Fig.2.

6. Step 3- Mathematical Modelling

At this step, a mathematical model was created, and its parameters were identified to map each fault signature to its releavnt location. A multi-layer-perceptron (MLP), as a type of artificial neural networks (ANNs), with a single hidden layer owning only sigmoid activation functions, (2), was opted as the mathematical model due to the following three reasons: (i) the model's mathematical form is unknown; therefore, a universal approximator should be used as the model. MLPs with a single hidden layer owning only sigmoid activation functions are universal approximators with a proven modelling capability [28]. (ii) MLPs, have been widely used to develop mathematical models for different purposes such as predictive modelling [29-31] and control [32-34]. (iii) Merit of MLPs in modelling with use of small number of data samples has been shown [35]. The inputs to the model, (2), are the elements of the fault signature, ${}_k\mathbf{M}_i$, and model's output is the estimated fault location, ${}_k\hat{y}$:

$$ {}_k\hat{y} = \sum_{j=1}^{h} \mathbf{T}_j f\left(\sum_{i=1}^{s} \mathbf{W}_{ij}\, {}_k\mathbf{M}_i + \mathbf{b}_j \right) + c. \quad (2)$$

where s is the number of model inputs or the size of fault signature, 24, ^ is used for the values estimated by the model. Eq.(3) demonstrates the utilised sigmoid function or f:

$$ f(x) = \frac{2}{1+\exp(-2x)} - 1 . \quad (3)$$

Research has shown that (3), also known as hyperbolic tangent function, outperforms many other well-known activation functions such as uni-polar and bi-polar sigmoid, conic section and radial basis function (RBF) in terms of proving the MLP with a higher recognition accuracy [36]. Therefore, (3) can be used as an activation function in most of MLP applications as an appropriate choice to obtain high accuracy [36].

Table II
First 10 natural frequencies and first 10 elements of the signature for the first fault location

Mode	Natural Freq. of Healthy Part (Hz)	Natural Freq. of Faulty Part (Hz)	Fault Signature (first 10 elements)
1	1234.4	1223.9	10.5
2	1660.3	1648.7	11.6
3	2364.6	2347.5	17.1
4	2705.0	2685.0	20
5	3068.3	3041.5	26.8
6	3579.5	3556.5	23
7	3655.7	3627.4	28.3
8	3736.2	3692.3	43.9
9	3749.3	3707.5	41.8
10	3787.4	3733.4	54.0

h, the number of neurons in the hidden layer, has been suggested to be calculated according to (4) in the literature, based on Kolmogorov's theorem [33, 37]:

$$h=2s+1. \quad (4)$$

That is, $h=49$. Hence, only unknown matrices/vectors/scalars are **W**, **T**, **b** and *c*. The elements of **W** and **T** are known as the weights of the first and the second layers of the MLP; **b** and *c* are called biases.

Aforementioned unknown parameters of the MLP were identified using the data presented in section 5. Parameter identification of an MLP consists of the following procedures: (i) initialisation and training, (ii) validation and (iii) test. Each needs a data series of its own. In this research, 14, 4 and 2 randomly chosen fault locations and their relevant fault signatures were used for initialisation/training, validation and test, respectively. These data are known as the training, the validation and the test data. The key idea of parameter identification is to decrease the error:

$$E=\frac{\sum_{\text{over designated data}}({}_k y-{}_k \hat{y})^2}{number\ of\ data\ samples}. \quad (5)$$

The error is named after the data set used for its calculation: training, validation or test. As this error uses the whole data set, any method using this error is a "batch" method.

At the beginning of parameter identification, initial values of unknown model parameters were estimated using Nguyen-Widrow algorithm [38], which is briefly presented in Appendix 1. Initialisation may need to be repeated as detailed in the pseudocode. Then, Levenberg-Marquardt error back propagation, introduced in Appendix 2, was employed to further tune unknown parameters of the model using the training data. The following pseudocode presents a summary of iterative parameter identification algorithm used in this research:

- Development of MLP structure based on (2) and (3)
- 10 Estimation of initial values of unknown parameters with Nguyen-Widrow algorithm
- *For i*=1:100
  - 20 Calculation of the training error (*TRE*) with use of (5) and the training data
  - 30 Tuning the values, calculated at the previous step, using batch Levenberg-Marquardt error back-propagation method and *TRE*
  - 40 Calculation of the validation error (*VE*) with use of (5) and the validation data
  - 50 *If VE*(*i*)>*VE*(*i*-1) *go to* 20
- 60 Calculation of the test error (*TSE*) based on (5) with the test data
- If *TSE* is unacceptable *go to* 10
- *End*

In the *For* loop of the pseudocode, the training error often continues to decrease while the validation error increases; this phenomenon is called overfitting which leads to the lack of generality of the model [39]. In this research, increase of the validation error, *VE*, triggers to stop the algorithm to prevent overfitting.

7. Results and Discussion

The accuracy of the developed fault isolation model was assessed with estimating two randomly selected fault locations, where none have been utilised neither in parameter identification (lines 10, 20 and 30 of the pseudocode) nor in validation of model (2) (lines 40 and 50 of the pseudocode) . The aforementioned two faults are located 7 cm and 14 cm away the origin, and their estimated locations by the model are 8.5 cm and 13.93 cm, respectively. Such satisfactory test results mean that the model is cross-validated in the operating area that its training, validation and test data have been gathered from.

As a major advantage of this approach, the employed modal information was collected at frequencies below 5 kHz, capturable by commercial sensors. That is, easy to collect vibrational information can be effectively used for fault isolation in complex automobile parts.

Although, the method was only adopted to isolate a fault on a line, the proposed methodology can be manifestly used to find two or three dimensions of a fault, providing that the results of adequate number of experiments or trustworthy numerical simulations are available. The number of required experiments/simulations can be reasonably considered related to the number of parameters (including both scalars and vector/matrix elements) of the model, Ψ. In model (2), **T** and **b** have *h* elements each, and **W** is of $s\times h$ elements. Therefore, the model has $\Psi=(s+2)h+1$ parameters.

So as to estimate a fault location with *d* dimensions, in which *d* is the dimension of fault location (2 or 3), model (2) of section 6 would be adapted to have *d* outputs. Based on Kolmogorov theorem [40], [33, 41] propose that the number of neurons in the hidden layer (*h*) are only contingent on the number of inputs as offered by (4). Therefore, *h* is identical for (2) and the models to estimate *d* dimensions of the fault location; hence, the size of **W** and **b** would not alter. However, the size of **T** would increase to $d\times h$, and *c* becomes a vector with the size of *d*. Hence, the number of parameter of an MLP model to estimate *d* dimensions of a fault location is $\Psi=(s+d+1)h+d$. Considering (4):

$$\Psi(d,s)=(s+d+1)(2s+1)+d. \quad (6)$$

For instance, with availability fault signatures with 24 elements or $s=24$, according to (6), the number of

parameters (or Ψ) of an MLP to estimate a fault location with one, two or three dimensions would be 1226, 1276 and 1326, respectively. The discrepancy is not substantial. Thus, the number of experiments/ numerical simulations required to develop a mathematical model to isolate faults in a two or three dimensional space would be only slightly greater than the number of experiments/ numerical simulations required to do the same task in a one dimensional space. Size (e.g. equivalent diameter) and shape factor may be considered as additional outputs too. In this case, d would equal 5. For s=24 and d=5, the number of model parameters, Ψ, would be 1426.

8. Conclusion

This article presents a new fault-diagnosis approach, suitable for mechanical components and structures with complex geometry, with use of easily measurable natural frequencies and an MLP mathematical model. The highlight of this work is to formulate the well-known problem of vibration-based structural health inspection in a way to be tackled by artificial intelligence methods. The proposed method was shown to be highly accurate to locate an under-surface fault in an automobile cylinder block. In order to develop the fault isolation algorithm for the aforementioned part, first, natural frequencies of a specimen with a fault were (numerically) obtained for a number of fault locations and deducted from the natural frequencies of the healthy part. The resultant, for each fault location, was named 'signature of the fault location' or 'fault signature'. Afterwards, an MLP was developed and identified using 14 and 4 different fault signatures and their relevant locations for training and validation, respectively. The developed model precisely estimates the location of fault in two faulty specimens in which their information were used neither in training nor in validation. This research evidently shows that the vibrational modal information, at low frequencies (below 5kHz for the investigated case study), can be sufficient for fault diagnosis of complicated mechanical parts, providing that this information is appropriately processed using effective data analysis algorithms.

References

[1] A. Glowacz, "Fault diagnosis of single-phase induction motor based on acoustic signals," *Mechanical Systems Signal Processing*, vol. 117, pp. 65-80, 2019.

[2] P. Jain, J. Poon, J. P. Singh, C. Spanos, S. R. Sanders, and S. K. Panda, "A Digital Twin Approach for Fault Diagnosis in Distributed Photovoltaic Systems," *IEEE Transactions on Power Electronics*, vol. 35, pp. 940-956, 2019.

[3] R. Xiong, Q. Yu, W. Shen, C. Lin, and F. Sun, "A sensor fault diagnosis method for a lithium-ion battery pack in electric vehicles," *IEEE Transactions on Power Electronics*, vol. 34, pp. 9709-9718, 2019.

[4] Q. Zhou, P. Yan, H. Liu, and Y. J. J. o. I. M. Xin, "A hybrid fault diagnosis method for mechanical components based on ontology and signal analysis," vol. 30, pp. 1693-1715, 2019.

[5] X. Li, Y. Yang, H. Shao, X. Zhong, J. Cheng, and J. Cheng, "Symplectic weighted sparse support matrix machine for gear fault diagnosis," *Measurement*, vol. 168, p. 108392, 2021.

[6] H. Hoshyarmanesh, M. Ghodsi, M. Kim, H. H. Cho, and H.-H. Park, "Temperature effects on electromechanical response of deposited piezoelectric sensors used in structural health monitoring of aerospace structures," *Sensors*, vol. 19, p. 2805, 2019.

[7] Z. Gao, C. Cecati, and S. X. Ding, "A survey of fault diagnosis and fault-tolerant techniques-Part I: fault diagnosis With model-based and signal-based approaches," *IEEE Transactions on Industrial Electronics*, vol. 62, pp. 3757-3767, 2015.

[8] M. Ghodsi, H. Ziaiefar, M. Amiryan, F. Honarvar, Y. Hojjat, M. Mahmoudi, *et al.*, "Lamb wave feature extraction using discrete wavelet transformation and Principal Component Analysis," in *Nondestructive Characterization and Monitoring of Advanced Materials, Aerospace, and Civil Infrastructure 2016*, 2016, p. 98041F.

[9] Y. Yan, L. Cheng, Z. Wu, and L. Yam, "Development in vibration-based structural damage detection technique," *Mechanical Systems and Signal Processing*, vol. 21, pp. 2198-2211, 2007.

[10] M. Mohammadzaheri, A. Akbarifar, M. Ghodsi, I. Bahadur, F. Al-Jahwari, and B. Al-Amri, "Health Monitoring of Welded Pipelines with Mechanical Waves and Fuzzy Inference Systems," presented at the International Gas Union Research Conference, Muscat, Oman, 2020.

[11] M. Taajobian, M. Mohammadzaheri, M. Doustmohammadi, A. Amouzadeh, and M. Emadi, "Fault diagnosis of an automobile cylinder head using low frequency vibrational data," *Journal of Mechanical Science and Technology*, vol. 32, pp. 3037-3045, 2018.

[12] K. Watanabe, I. Matsuura, M. Abe, M. Kubota, and D. Himmelblau, "Incipient fault diagnosis of chemical processes via artificial neural networks," *AIChE journal*, vol. 35, pp. 1803-1812, 1989.

[13] S. Nandi, H. Toliyat, and X. Li, "Condition monitoring and fault diagnosis of electrical motors-a review," *IEEE Transactions on Energy Conversion,*, vol. 20, pp. 719-729, 2005.

[14] M. Silva, A. Santos, and E. Figueiredo, "Damage Detection for Structural Health Monitoring of Bridges as a Knowledge Discovery in Databases Process," in *Data Mining in Structural Dynamic Analysis*, ed: Springer, 2019, pp. 1-24.

[15] C. R. Farrar and S. W. Doebling, "An overview of modal-based damage identification methods," in *Proceedings of DAMAS Conference*, 1997, pp. 269-278.

[16] S. Wang, M. Lian, S. Zhou, J. Feng, and Y. Rao, "Research and Outlook on Leak Detection Technology of Natural Gas Pipelines," presented at the International Conference on Pipelines and Trenchless Technology, Wuhan, China, 2012.

[17] M. Yoon, D. Heider, J. Gillespie, C. Ratcliffe, and R. Crane, "Local damage detection using the two-dimensional gapped smoothing method," *Journal of Sound and Vibration*, vol. 279, pp. 119-139, 2005.

[18] S. Hakim, H. A. Razak, and S. Ravanfar, "Fault diagnosis on beam-like structures from modal parameters using artificial neural networks," *Measurement*, vol. 76, pp. 45-61, 2015.

[19] D. Hunt, S. Weiss, W. West, T. Dunlap, and S. Freesmeyer, "Development and implementation of a shuttle modal inspection system," in *International Modal Analysis Conference, 8 th, Kissimmee, FL*, 1990, pp. 919-925.

[20] M.-B. Abdo and M. Hori, "A numerical study of structural damage detection using changes in the rotation of mode shapes," *Journal of Sound and vibration*, vol. 251, pp. 227-239, 2002.

[21] K. Aydin and O. Kisi, "Applicability of a Fuzzy Genetic System for Crack Diagnosis in Timoshenko Beams," *Journal of Computing in Civil Engineering*, 2014.

[22] S. W. Doebling, C. R. Farrar, and M. B. Prime, "A summary review of vibration-based damage identification methods," *Shock and vibration digest*, vol. 30, pp. 91-105, 1998.

[23] P. Soltani, M. Keikhosravy, R. Oskouei, and C. Soutis, "Studying the tensile behaviour of GLARE laminates: a finite

element modelling approach," *Applied Composite Materials*, vol. 18, pp. 271-282, 2011.
[24] I. D. Landau and G. Zito, *Digital Control Systems*: Springer London, 2006.
[25] A. Akbarifar, M. Mohammadzaheri, A. Joudaki, E. Jamshidi, S. Khabbaz, M. Parmoon, *et al.*, "Fault Detection of Gas Pipelines Using Mechanical Waves and Intelligent Techniques," presented at the International Conference on Artificial Intelligence, Energy and Manufacturing Engineering Dubai, UAE, 2015.
[26] Q. Xu, "Minimal Structural ART Neural Network and Fault Diagnosis Application of Gas Turbine," *The Open Mechanical Engineering Journal*, vol. 10, 2016.
[27] S. Shabestari, M. Rahmani, S. Saeedinia, and O. Lashgari, "Influence of Metalurgical Processes on Structure and Mechanical Characteristics of Paykan 1600 Aluminum Cylinder Head," presented at the The First Iranian Symposium of Internal Combustion Enginers, Tehran, Iran, 1999.
[28] T. P. Chen, H. Chen, and R. W. Liu, "Approximation capability in C(R˜N) by multilayer feedforward networks and related problems," *IEEE Transactions on Neural Networks*, vol. 6, pp. 25-30, Jan 1995.
[29] M. Mohammadzaheri and L. Chen, "Intelligent modelling of MIMO nonlinear dynamic process plants for predictive control purposes," in *Proceedings of the 17th World Congress The International Federation of Automatic Control Seoul, Korea*, 2008, pp. 12401-12406.
[30] M. Mohammadzaheri, R. Tafreshi, Z. Khan, M. Franchek, and K. Grigoriadis, "Modelling of Petroleum Multiphase Fluids In ESP an Intelligent Approach," in *Offshore Mediterranean Conference and Exhibition*, 2015.
[31] M. Bazghaleh, M. Mohammadzaheri, S. Grainger, B. Cazzolato, and T. F. Lu, "A new hybrid method for sensorless control of piezoelectric actuators," *Sensors and Actuators A: Physical*, vol. 194, pp. 25-30, 2013.
[32] M. Mohammadzaheri, L. Chen, A. Mirsepahi, M. Ghanbari, and R. Tafreshi, "Neuro-Predictive Control of an Infrared Dryer with a Feedforward-Feedback Approach," *Asian Journal of Control*, vol. 17, pp. 1972-1977, 2015/9/1 2015.
[33] M. Mohammadzaheri, L. Chen, and S. Grainger, "A critical review of the most popular types of neuro control," *Asian Journal of Control*, vol. 16, pp. 1-11, 2012.
[34] M. Mohammadzaheri and L. Chen, "Intelligent predictive control of a model helicopter's yaw angle," *Asian Journal of Control*, vol. 12, pp. 667-679, 2010.
[35] M. Mohammadzaheri, H. Ziaeifar, I. Bahadur, M. Zarog, M. Emadi, and M. Ghodsi, "Data-driven Modelling of Engineering Systems with Small Data, a Comparative Study of Artificial Intelligence Techniques," in *2019 5th Iranian Conference on Signal Processing and Intelligent Systems (ICSPIS)*, 2019, pp. 1-5.
[36] B. Karlik and A. V. Olgac, "Performance analysis of various activation functions in generalized MLP architectures of neural networks," *International Journal of Artificial Intelligence and Expert Systems*, vol. 1, pp. 111-122, 2011.
[37] R. Hecht-Nielsen, "Kolmogorov's mapping neural network existence theorem," in *Proceedings of the international conference on Neural Networks*, 1987, pp. 11-14.
[38] D. Nguyen and B. Widrow, "Improving the learning speed of 2-layer neural networks by choosing initial values of the adaptive weights," presented at the International Joint Conference on Neural Networks, 1990.
[39] D. Bhattacharyay, D. Kocaefe, Y. Kocaefe, and B. Morais, "An artificial neural network model for predicting the CO 2 reactivity of carbon anodes used in the primary aluminum production," *Neural computing and Applications*, vol. 28, pp. 553-563, 2017.
[40] V. Kůrková, "Kolmogorov's theorem and multilayer neural networks," *Neural networks*, vol. 5, pp. 501-506, 1992.
[41] S. Haykin, *Neural Networks A Comprehensive Introduction*: Prentice Hall, New Jersey, 1999.
[42] D. Nguyen and B. Widrow, "Improving the learning speed of 2-layer neural networks by choosing initial values of the adaptive weights," in *Neural Networks, 1990., 1990 IJCNN International Joint Conference on*, 1990, pp. 21-26.
[43] M. Mohammadzaheri, R. Tafreshi, Z. Khan, M. Franchek, and K. Grigoriadis, "An intelligent approach to optimize multiphase subsea oil fields lifted by electrical submersible pumps," *Journal of Computational Science*, vol. 15, pp. 50-59, 2016.
[44] M. Mohammadzaheri, R. Tafreshi, Z. Khan, M. Ghodsi, M. Franchek, K. J. S. Grigoriadis, *et al.*, "Modelling of petroleum multiphase flow in electrical submersible pumps with shallow artificial neural networks," vol. 15, pp. 174-183, 2020.
[45] J. R. Jang, C. Sun, and E. Mizutani, *Neuro-Fuzzy and Soft Computing*. New Delhi: Prentice-Hall of India, 2006.

APPENDIX A1. A BRIEF INTRODUCTION TO NGUYEN-WIDROW PARAMETER INITIALISATION ALGORITHM

Fig.A.1 depicts the sigmoid activation function of (3). This function is almost linear within an interval; the slope of the functions decreases towards zero, as it goes further than this interval.

Practically, if the input to a sigmoid activation function is located outside the range relevant to the linear interval, the function is of trivial effect on the model output, and accordingly, on the error and parameter identification algorithm. Such an event decelerates MLP parameter identification. Nguyen-Widrow algorithm estimates initial values of the model parameters, so that the outputs of the activation functions (for the training data) are situated within their linear intervals [42, 43].

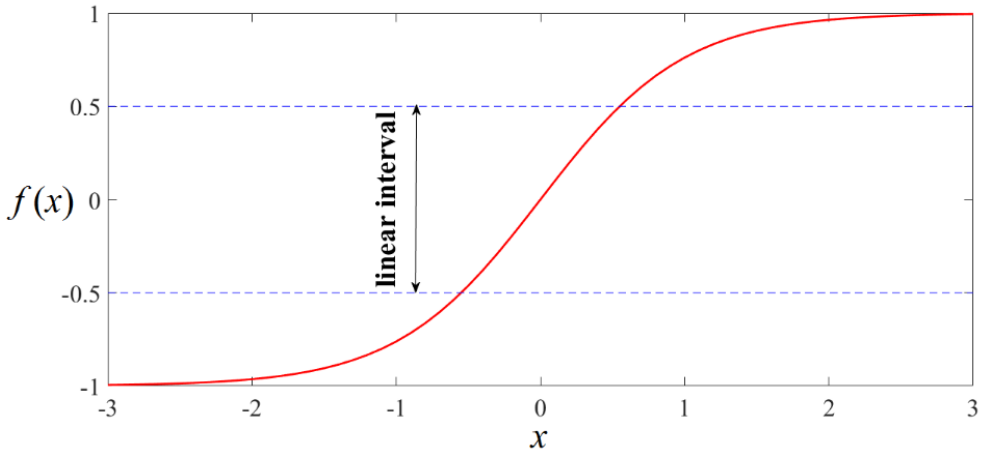

Fig. A.1. The sigmoid activation function of (3) and its linear interval

As a disadvantage, all derivative-based optimisation algorithms, e.g. Levenberg-Marquardt used in this research to tune the MLP parameters, may be caught in a local minimum of error. That is, the training process leads to an inaccurate MLP with a considerable estimation error. With restart of training from the identical initial values of parameters, the model is again caught at the same trap.

Therefore, the initialisation algorithm should produce different initial values for the MLP parameters in every run. To do so, this algorithms includes random functions [44].

APPENDIX A2. LEVENBERG-MARQUARDT METHOD

The error or E of (5) can be presented as $E(\boldsymbol{\theta})$, where $\boldsymbol{\theta}$ is a vector of entire MLP parameters. Tuning of $\boldsymbol{\theta}$ elements (from their initial values) to minimise $E(\boldsymbol{\theta})$ for the training data. An approach to tackle this optimisation problem is to approximate the error function with a second order Taylor series:

$$E(\boldsymbol{\theta}+\Delta\boldsymbol{\theta}) \cong E(\boldsymbol{\theta}) + \frac{\partial E(\boldsymbol{\theta})}{\partial \boldsymbol{\theta}}(\Delta\boldsymbol{\theta}) + \frac{1}{2}\frac{\partial^2 E(\boldsymbol{\theta})}{\partial \boldsymbol{\theta}^2}(\Delta\boldsymbol{\theta})^2. \quad \text{(A.1)}$$

This approximation is aimed to determine $\Delta\boldsymbol{\theta}$ so as to (almost) assure that the error decreases. The following is the derivative of the error respect to $\boldsymbol{\theta}$:

$$\frac{\partial E(\boldsymbol{\theta})}{\partial \boldsymbol{\theta}} = \mathbf{g} = \left[\frac{\partial E(\boldsymbol{\theta})}{\partial \theta_1}, \cdots, \frac{\partial E(\boldsymbol{\theta})}{\partial \theta_{n_p}}\right]^T.$$

$$\frac{\partial^2 E(\boldsymbol{\theta})}{\partial \boldsymbol{\theta}^2} = \mathbf{H} = \begin{bmatrix} \frac{\partial^2 E(\boldsymbol{\theta})}{\partial \theta_1^2} & \frac{\partial^2 E(\boldsymbol{\theta})}{\partial \theta_1 \partial \theta_2} & \cdots & \frac{\partial^2 E(\boldsymbol{\theta})}{\partial \theta_1 \partial \theta_{n_p-1}} & \frac{\partial^2 E(\boldsymbol{\theta})}{\partial \theta_1 \partial \theta_{n_p}} \\ \vdots & & \ddots & & \vdots \\ \frac{\partial^2 E(\boldsymbol{\theta})}{\partial \theta_{n_p} \partial \theta_1} & \frac{\partial^2 E(\boldsymbol{\theta})}{\partial \theta_{n_p} \partial \theta_2} & \cdots & \frac{\partial^2 E(\boldsymbol{\theta})}{\partial \theta_{n_p} \partial \theta_{n_p-1}} & \frac{\partial^2 E(\boldsymbol{\theta})}{\partial \theta_{n_p}^2} \end{bmatrix},$$

where n_p is the number of parameters. (A.2) is a solution to this optimisation, known as Newton direction [45]:

$$\Delta\boldsymbol{\theta} = -\mathbf{H}^{-1}\mathbf{g}. \quad \text{(A.2)}$$

Nevertheless, (A.2) is of use only in the case of inevitability of H . Levenberg and Marquardt [45] suggested an alternative to address this shortcoming(A.2):

$$\Delta\boldsymbol{\theta} = -\eta(\mathbf{H}+\lambda\mathbf{I})^{-1}\mathbf{g}. \quad \text{(A.3)}$$

where $\mathbf{I}$ is the unit matrix with the size of n_p , and λ is the minimum number that can make $\mathbf{H}+\lambda\mathbf{I}$ invertible; linear search may be used to determine η. Details of algorithms to determine η and λ are available in[34, 45]. Prior to finding the values of $\mathbf{H}$ and $\mathbf{g}$ elements, E and its derivatives need to be analytically presented as functions of $\boldsymbol{\theta}$. Development of such a presentation is known as error back-propagation.